Computationally Modeling Spreading Depolarizations' Impact on Intrinsic Patterns of Brain Activity

A Technical Report submitted to the Department of Biomedical Engineering

Presented to the Faculty of the School of Engineering and Applied Science
University of Virginia • Charlottesville, Virginia

In Partial Fulfillment of the Requirements for the Degree
Bachelor of Science, School of Engineering

Lex Fedor
Spring, 2025

On my honor as a University Student, I have neither given nor received unauthorized aid on this assignment as defined by the Honor Guidelines for Thesis-Related Assignments

Andrew Carlson, Department of Neurosurgery

Computationally Modeling Spreading Depolarizations' Impact on Intrinsic Patterns of Brain Activity

Lex Fedor[a], Andrew Carlson[1]

[a] Department of Biomedical Engineering, University of Virginia

[1] Correspondence: EQB2TS@uvahealth.org

Abstract

Spreading depolarizations (SDs) are pathologic periods of brain activity suppression that travel at a rate of 2-5 mm/min and last several minutes[1]. During these several minutes, neuronal dysfunction can occur which may lead to delayed cerebral ischemia (DCI) or worsening of prognosis. There is little known about the effects that SD has on brain activity. Thus, using metrics such as the alpha-delta power ratio (ADR) to determine ischemic risk and cross-frequency coupling (CFC) metrics such as the modulation index (MI), phase-locking value (PLV), and the amplitude-envelop correlation (r_{AEC}) to determine neuronal dysfunction, SD impact on brain activity can be quantified. Two de-identified electrocorticography (ECoG) datasets (one bypass patient and one stroke patient) were used to calculate these metrics. It was found that the ADR did not corroborate past studies as it increased in value during SD onset rather than decrease. Additionally, MI was found to change the most when the delta phase was used with the theta and alpha amplitude, regardless of SD presence. PLV was found to change the most when the high gamma (HG) or the delta phase were impacted. r_{AEC} was found to change the most when the gamma amplitude was impacted and the theta, alpha, or beta amplitude was not impacted. Overall, there was a loose correlation for all coupling metrics between SD duration and percent change between before and during SD onset. The longer the SD was, the greater the metric became during SD onset. Further studies on different correlations such as SD amplitude as well as different injury types must be done in order to fully understand the effect SDs have on the brain.

Keywords: Spreading depolarization, alpha delta ratio, cross-frequency coupling

Introduction

SDs, or more colloquially known as brain tsunamis, are propagating waves of depolarization that result in cortical activity suppression that lasts several minutes at a time. SDs are characterized by a sharp negative DC shift that occurs closely to high frequency activity suppression. SDs have been reported to occur in acute stroke, subarachnoid hemorrhages (SAH), acute traumatic brain injury (TBI), and migraines[1,2]. In the past, SDs have gone under the radar due to similarities in quality with artifacts in scalp electroencephalography (EEG). With better technology and more specificity, ECoG has made SDs easier to identify at the cost of an invasive craniotomy or burr holes in the skull. With electrodes directly on the surface of the brain, artifacts and SDs are much more distinguishable, making SDs much easier to study.

Many studies focus on effects that SD has on cerebral blood flow or cellular changes as a whole, but not much is said about the effects SD have on individual brain frequencies[3–5]. During SD, it's postulated that the SD wave allows for the disinhibition of the NMDA receptor due to the absence of magnesium which leads to increased sensitivity to glutamate levels, triggering the release of potassium and excitatory amino acids[1]. As SD propagates, cytotoxic oedema can occur due to the increased water uptake into the neuron. The impacted brain area enters a hyperemic phase where the cerebral blood flow has been shown to increase 100%-200% before plummeting to 20%-30% of the baseline. The recovery period of the suppression due to SD is roughly 5-15 minutes whereas the blood flow reduction lasts for 1-2 hours[6].

Acknowledging the effects that SDs can have on ischemic risk or overall neuronal dysfunction is incredibly important to better understand how SDs affect the brain. Various methods of quantification can be used to mathematically describe dysfunction of communication between neurons. Delta, theta, and gamma are often the most studied due to their implications in consolidation, memory, and executive functions[7]. Quantifying the effect that SD has on these across time and space may bring light to the impact that SDs have on the brain.

ADR has been used in the past to predict DCI. Traditionally, ADR has been studied using quantitative or continuous EEG on SAH patients. DCI on its own is complicated and not fully understood allowing it to go unrecognized. It is common and brings about its own complications that are disabling, typically 4-14 days after onset. Many studies use various metrics to predict DCI such as delta-alpha power ratio, (delta + theta)/(alpha + beta) power ratio, relative delta power, relative alpha power variability, as well as ADR[8,9]. ADR was chosen due to its strong linkage with DCI. Worsening ADR has been reported to be 80% sensitive and 27% specific in a sample size of 95 aneurysmal SAH patients using automated EEG[10] and a higher reported sensitivity of 95% and specificity of 77% in a sample size of 103 high baseline risk SAH patients using quantitative EEG[8]. These metrics can be specific and

sensitive to ischemic stroke as abnormal slow EEG activity within the delta range and attenuation of faster activity within the alpha range occurs during onset[11].

CFC metric calculations allow for the quantification of slow wave encoding of temporal information with the rhythmic spiking activity of the fast oscillation to quantify neuronal communication. However, CFC is incredibly vulnerable to fluctuations and bias[7]. Aru et al. speaks on ways to circumvent these biases, one of which is by using healthy or surrogate data[12]. CFC can be split up into different types such as phase-amplitude coupling (PAC) and amplitude-amplitude coupling (AAC). Theta-gamma coupling is the main PAC that is observed as it occurs during wakefulness, information encoding, working memory, retrieval, and sleep[13]. More generically, PAC quantifies the modulation of the high frequency amplitude oscillation with the slow frequency phase oscillation[14]. Two methods of quantifying PAC were used: modulation index (MI), which typically correlates high frequency oscillations (HFOs) amplitude with low frequency oscillations (LFOs) phases, and phase-locking value, which correlates one phase to another phase. For MI, the higher the value the greater the PAC whereas for the PLV a 1 represents perfect phase locking. AAC is far less studied than other forms of CFC. However, one form of AAC is the amplitude-envelope correlation (r_{AEC}), used to quantify how temporally correlated two amplitude envelopes are[15].

Thus, ADR and CFC should both decrease during SD onset and return to baseline within a couple hours. CFC may be more informative as it is more generalizable to neuronal dysfunction where ADR is specific to DCI.

Results

SD Identification

Two de-identified ECoG datasets, one from a patient with a bypass and one from a stroke patient, were used in this study. Twenty-nine SDs were found for the bypass patient and twenty-one were found for the stroke patient. The electrodes that were impacted by the SD were subsequently called the impacted electrodes, whereas the electrodes that did not experience an SD were called the adjacent electrodes. For the stroke patient, many of these SDs occurred during the same period of suppression but were counted individually. The identified SDs experienced by the bypass patient were both longer in duration and of greater peak amplitude, though no significant differences were found (Figure 1). In an attempt to evade artifacts, the median was used for all calculations other than the SD duration and peak SD amplitude as those were guaranteed to be without artifact.

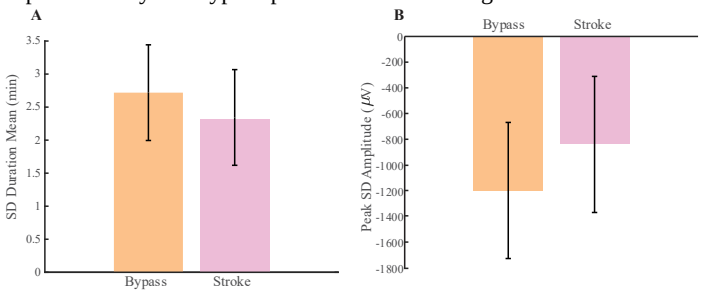

Fig. 1. SD Duration and Peak Amplitude. A) Median SD duration for all SD for both patients is shown. B) Median peak SD amplitude for all SD for both patients is shown.

Furthermore, looking at the normalized relative power of each wavelength shows that the relative power of most all wavelengths are negative for the stroke patient whereas the bypass patient has far more variation (Figure 2). Additionally, during SD onset, the relative power is more affected in the stroke patient as seen by the clustering (Figure 2E). After SD onset, the bypass shows an impact on the alpha and beta relative power, whereas the stroke patient shows an impact on the delta and theta relative power (Figure 2C, F).

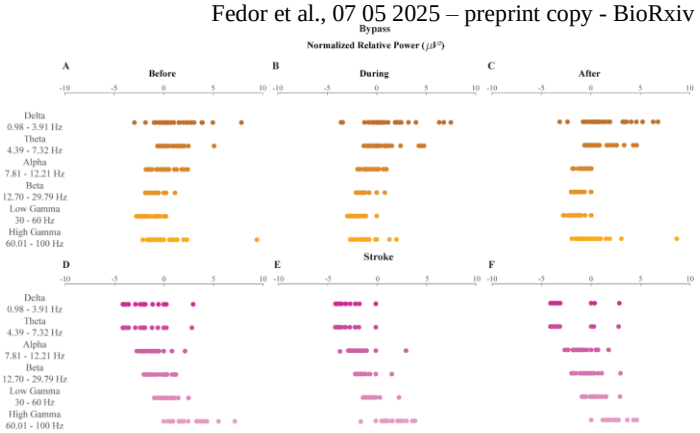

Fig. 2. Normalized Relative Power. Relative power for each frequency range before during and after are shown for the bypass patient (A-C) and the stroke patient (D-F).

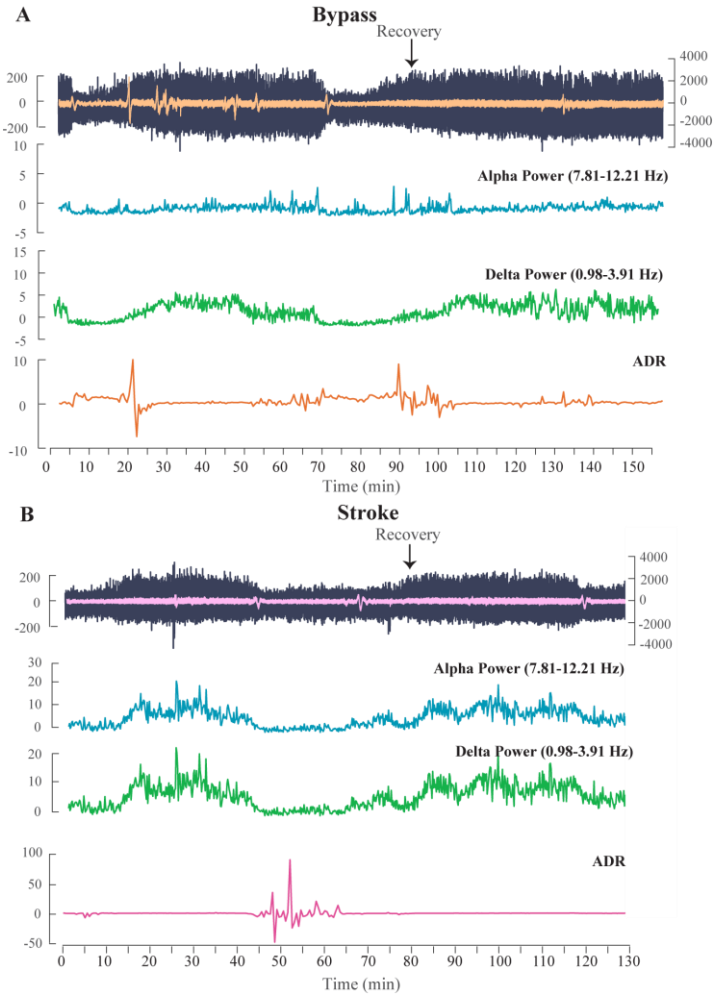

Fig. 3. ADR Time Series. A) Bypass patient ADR is shown to increase during SD onset and returns to baseline several minutes after suppression recovery. B) Stroke patient ADR is shown to increase during SD onset and returns to baseline shortly before suppression recovery.

ADR

SDs are shown to impact ADR throughout high frequency suppression (Figure 3). Delta power is visibly affected during suppression for both patients. The presence of multiple SDs during one period of suppression does not seem to impact the longevity of ADR disruption (Figure 3B).

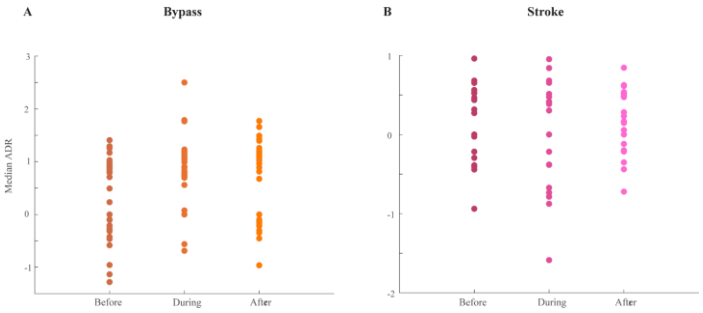

Fig. 4. ADR Distribution Overview. A) Bypass patient median ADR is shown to increase during SD onset before returning to similar values as before SD onset. B) Stroke patient median ADR is shown be resistant to change save for a possible outlier. After SD resolves, the median ADR reduces compared to during SD onset but is not dissimilar to the median ADR before SD onset.

Across all SDs, the median ADR during SD onset congregated closer together for the bypass patient whilst the opposite occurred for the stroke patient (Figure 4). After SD onset, the median ADR returned to a similar distribution and range as before SD onset for both patients. The correlation between SD duration and percent ADR change showed opposing regression lines across time comparisons and across patients (Figure 5). The bypass patient had a stronger correlation overall.

When comparing before SD onset median ADR values to those during SD onset for the bypass patient, there exist several values that show nearly no change in median ADR despite the duration of SD (Figure 5A). The same comparison for the stroke patient shows similar results, with several values showing little to no difference between time groups (Figure 5C). Despite both showing some relation between SD duration

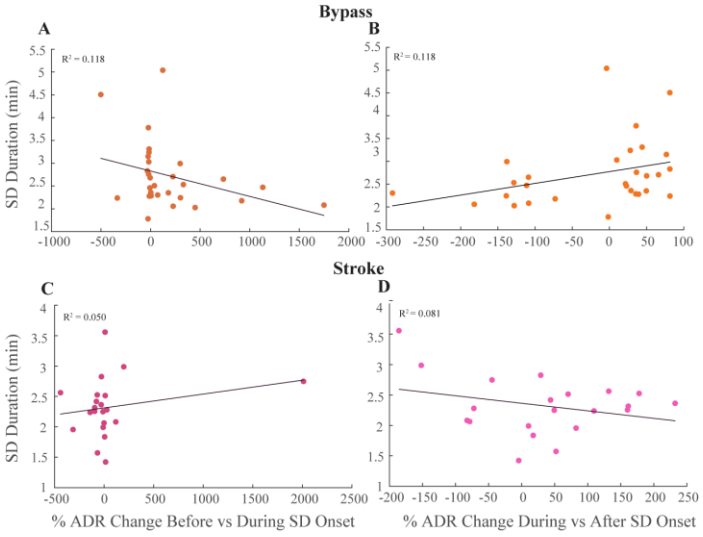

Fig. 5. ADR Regression. Bypass patient shows a negative correlation between SD duration and percent change before and during SD onset and a positive correlation between SD duration and percent change during and after SD onset (A-B). Stroke patient shows the opposite correlation trend (C-D). Neither patient shows strong correlation for any time comparison.

and ADR change, there is little confidence in the fit both due to the low R^2 values and the SD duration independent clustering. The comparison between during SD onset and after SD onset median ADR values show more duration dependent correlations for both patients (Figure 5B & 5D). For the bypass patient, as the SD duration decreases, the more negative of a change (or the smaller the median ADR is after SD onset). The opposite is true for the stroke patient, however, the R^2 is much lower.

Cross-Frequency Coupling

Modulation Index

MI shows little changes over time groups. The wavelength combinations that utilize the delta phase and the theta or alpha amplitude

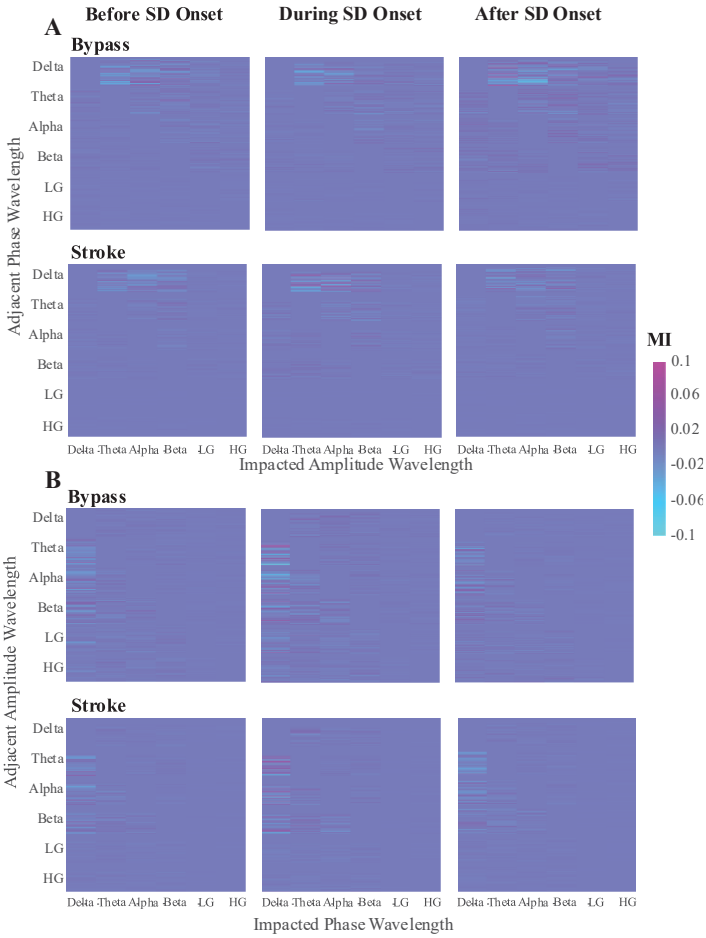

Fig. 6. MI Heatmap. Subtle differences in MI are shown for both patients across time. When the amplitude is impacted, the adjacent delta phase shows the highest magnitude of MI (A). Similarly, when none of the amplitudes are impacted the highest magnitude of MI shows when the delta phase is impacted (B).

show the greatest MI magnitude, regardless of whether the wavelengths used were on the impacted electrode or not (Figure 6). Visually, the impacted phase has a greater effect on the reported MI during SD for both patients. Interestingly, when the alpha amplitude is impacted rather than the delta phase for the bypass patient, there was a large visible decrease in MI after SD onset shown by the brighter blue presence in the heatmap (Figure 6A). For all other heatmap comparisons, the major MI change happened during SD onset. Additionally, the stroke patient experienced an increase in MI during SD onset whereas the bypass experienced a decrease (Figure 6B).

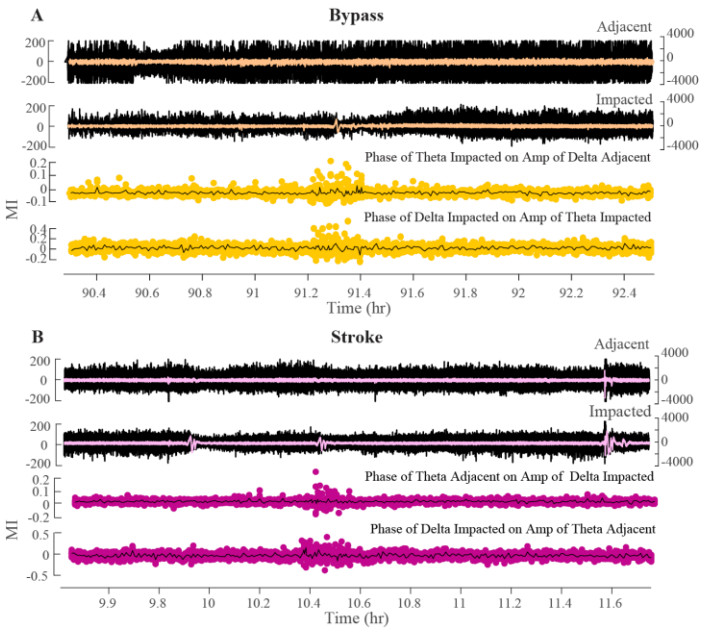

Fig. 7. MI Time Series. MI is shown to be disrupted during SD onset for both patients.

Representative time series data of the impacted delta phase and adjacent theta amplitude show visible disruption of the MI during SD onset (Figure 7). Rather than a uniform change in MI, the disruption comes by the way of increased variation in MI, though most of the change was positive. The bypass patient shows a small period of suppression with no SD on the adjacent electrode and shows no visible subsequent disruption of MI (Figure 7A). The stroke patient shows two SDs with small periods of suppression on the impacted electrode and only the second SD that occurs immediately after recovery shows a disruption of MI (Figure 7B).

Despite the greater visual disturbance seen in both the heatmap and the time series data, very little correlation is seen between the percent MI change and the duration of SD (Figure 8A-H). The outliers seen can possibly be due to the amateur identification of SD, biological randomness, or an unknown event that heavily impacted brain activity. There was little to no difference in the MI between before and after SD onset when the alpha amplitude was impacted for either patient. The impacted delta phase produced similar results for both patients and for both theta and alpha amplitude (Figure 8B, D, F, H). However, the stroke patient showed more variation when the alpha amplitude was used to calculate MI (Figure 8H). The impacted theta amplitude showed the most variation for both patients.

When looking at the difference in MI after SD resolves, the trends seen are not dissimilar to those at SD onset (Figure 9I-P). For the stroke patient, there is semblance of a correlation between SD duration and percent MI change after SD onset when the delta phase is impacted and the alpha amplitude is not (Figure 9H). However, none of the correlations shown are strong.

Phase-Locking Value

The PLV shows very little difference between patients nor time groups. The highest PLV values are reported when either the delta phase or the HG phase are used, regardless of whether these are on the impacted electrode (Figure 10).

Similarly to the MI heatmaps in Figure 6, there is very little visible disturbance in PLV for either patient. However, some suppression can be seen for the bypass patient when the delta phase is on the adjacent electrode and the HG phase is on the impacted electrode (Figure 11A). There is also some disturbance in the PLV for the stroke patient around

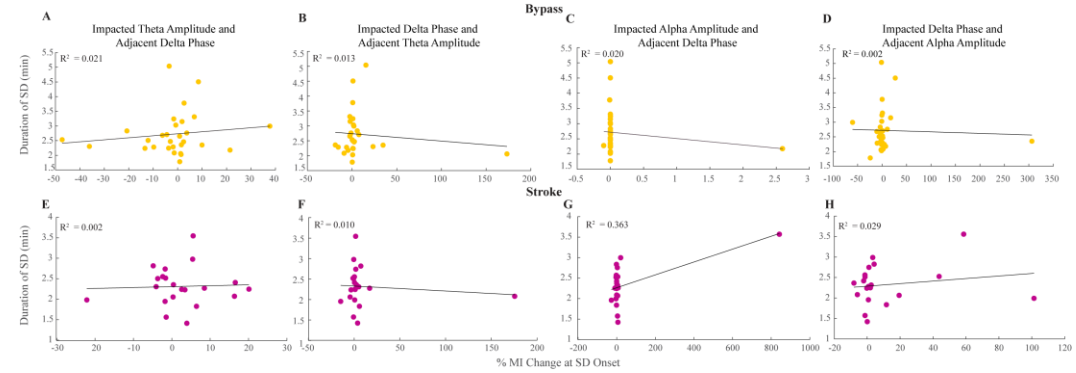

Fig. 8. MI Regression Before versus During SD Onset. Correlation between SD duration and percent MI change at SD onset is minimal. There is very little change in MI for many wavelength combinations (B-D & F-H). There exists some correlation when the theta amplitude is impacted and the delta phase isn't, but it is minimal. Little difference is shown between bypass patient and stroke patient.

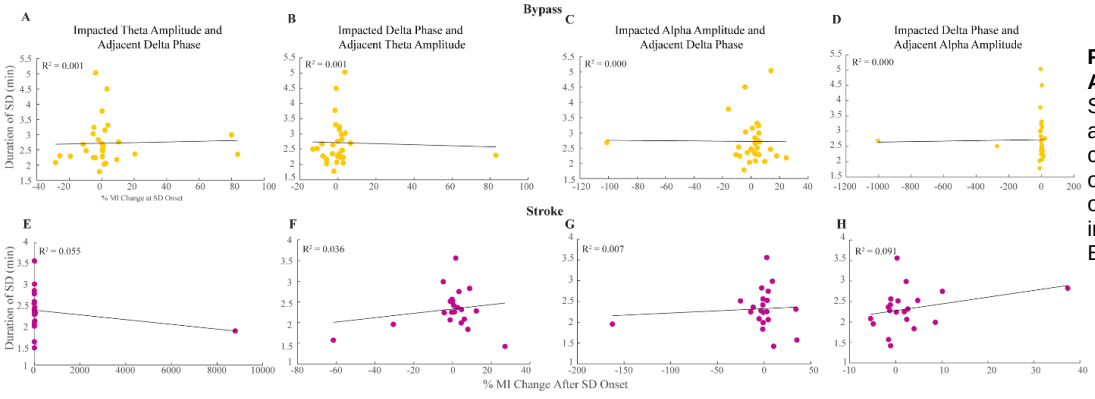

Fig. 9. MI Regression During versus After SD Onset. Correlation between SD duration and percent MI change after SD Onset shows minimal correlation. There is more of an effect on MI by SD than there was at SD onset. However, there are still many instances of very little MI change (D-E).

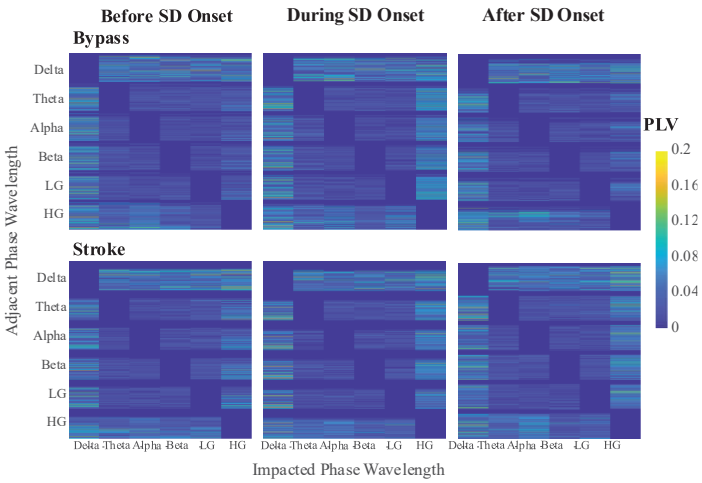

Fig. 10. PLV Heatmap. PLV is shown to be highest when high gamma (HG) and delta phase are used.

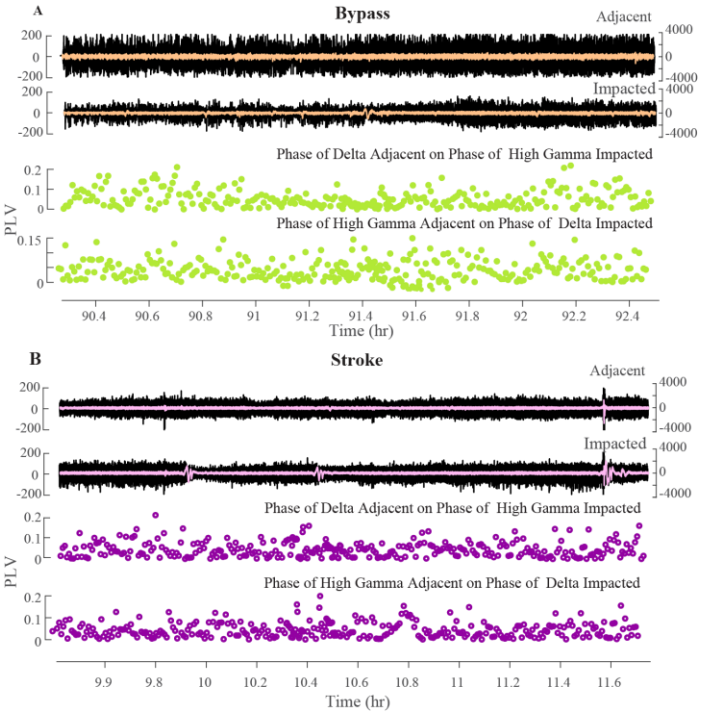

Fig. 11. PLV Time Series. PLV is seemingly affected by SD but the visual effect is minor. A) PLV visibly decreases around the time frame of the SD and doesn't increase until well several minutes after suppression resolves. B) There are two periods of PLV decreasing that are likely related to the presence of SD.

hour 10.8 when the HG phase is on the impacted electrode and the delta phase is on the adjacent electrode (Figure 11B). However, the correlation between this disturbance and the presence of the SD is hard to justify.

Despite the lack of visual differences in PLV for either patient, the regression plots show some correlation between the duration of SD and the percent change of PLV before and during SD onset (Figure 12). The bypass patient shows a loose positive correlation and the stroke patient shows little correlation. The longer the SD duration, the greater the calculated PLV was during SD onset.

After SD resolves, the correlation between the duration of SD and percent change between during SD onset and after is higher for both

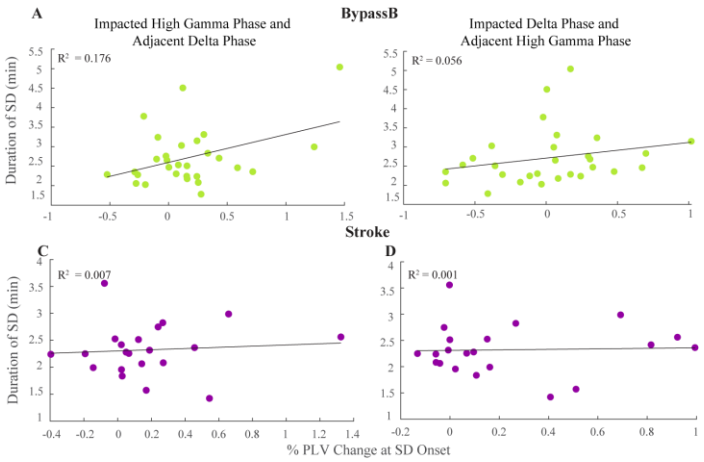

Fig. 12. PLV Regression Before versus During SD Onset. A) PLV shows a positive correlation for the bypass patient. B) The correlation is much weaker for the stroke patient and is far more horizontal.

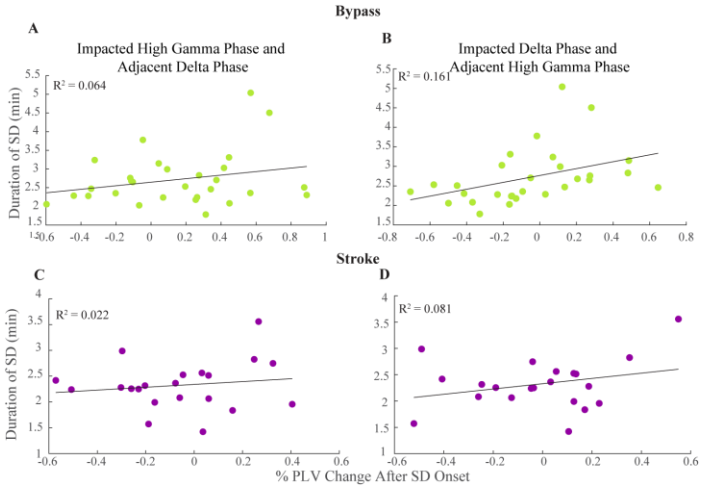

Fig. 13. PLV Regression During versus After SD Onset. A) PLV shows a positive correlation for the bypass patient. B) PLV shows a positive correlation for the stroke patient.

patients (Figure 13). Both patients show a positive correlation, indicating that the longer the SD duration, the greater the PLV was during SD propagation than after recovery. The bypass patient shows the highest correlation when the delta phase is impacted and the HG phase is not (Figure 13B). This directly contrasts the correlation present for the percent change at SD onset (Figure 12B). However, the percent change at SD onset had more variation surrounding the trendline.

Amplitude-Envelope Correlation

The low gamma (LG) and HG amplitude on the impacted electrode reports the highest r_{AEC} values for both patients (Figure 14). The most change in r_{AEC} across time groups for the bypass patient is when the alpha and beta amplitudes on the adjacent electrode are used. For the stroke patient, the theta, alpha, and beta show the most change across time groups. The stroke patient shows the higher r_{AEC} overall, indicating a higher correlation between amplitude envelopes than the bypass patient. The bypass patient shows a disturbance that seemingly simultaneously increases and decreases the r_{AEC} during SD onset. Contrarily, the stroke patient shows an increase in r_{AEC} during SD onset.

The r_{AEC} visibly increases during and after periods of suppression for both patients (Figure 15). There is little visible effect when the alpha amplitude is impacted for the bypass patient (Figure

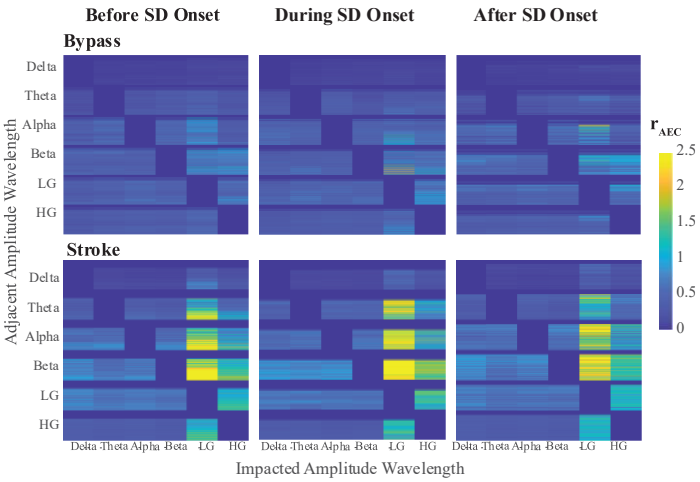

Fig. 14. r_{AEC} Heatmap. r_{AEC} is shown to be highest when the LG and high gamma amplitudes are impacted. Stroke patient shows the highest correlation values overall.

15A). The effect of the impacted alpha amplitude is subtle for the stroke patient but is still visible (Figure 15B). Additionally, the effect on r_{AEC} isn't seen until after SD resolves (Figure 15A). For the stroke patient, the presence of multiple SDs doesn't seem to cause higher r_{AEC} values. Additionally, the numerous negative DC shifts that occur independently of the high frequency activity suppression seemingly do not affect the r_{AEC} when the LG amplitude is impacted but does have an effect when the alpha amplitude is impacted (Figure 15B).

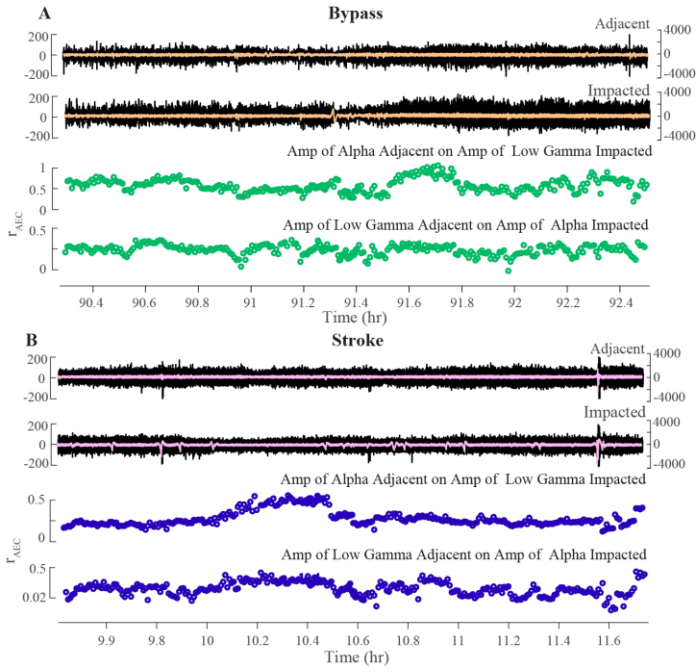

Fig. 15. r_{AEC} Time Series. r_{AEC} is shown to increase after SD onset. A) r_{AEC} increases drastically when the LG amplitude is impacted for the bypass patient. B) r_{AEC} increases no matter which amplitude is impacted. However, there is a much bigger increase when the LG amplitude is impacted.

Despite the visible disruption in r_{AEC} seen in Figure 15, the impacted LG amplitude does not show high correlation when its coupling with the adjacent alpha amplitude is assessed. Instead, there is higher correlation between the impacted HG amplitude and the adjacent alpha amplitude (Figure 16). Even so, the bypass patient shows very little correlation between SD duration and percent change in r_{AEC} between before and during SD onset except when the LG amplitude is impacted and the beta amplitude is not (Figure 16B). The stroke patient shows some correlation as well when the LG amplitude is impacted and the beta amplitude is not (Figure 16F). They also show some correlation when the HG amplitude is impacted, and the alpha amplitude is not (Figure 16G).

After SD resolves, there is much higher correlation between duration of SD and the percent change (Figure 17). However, the stroke patient has many outliers that skew the trendline and discount validity of the correlation. The bypass patient shows less correlation when the HG amplitude is impacted and the beta amplitude is not (Figure 17D). The stroke patient shows very little correlation when the LG is impacted (Figure 17E-F). The trendline for the stroke patient is riddled with outliers indicating that there is no real correlation between SD duration and percent change in r_{AEC} after SD onset (Figure 17E-H).

Discussion

The ADR and PAC metrics were predicted to decrease during SD onset before returning to normal. However, these metrics either increased or showed no difference. Additionally, it was purported that the longer the SD duration the greater the difference in metric during SD onset. This also was not fully seen in any of the metrics. Some loose correlation existed showing the longer the SD duration, the greater the metric was during onset.

Worsening ADR is known to be a reliable predictor of DCI in patients with aneurysmal SAH. In this study, the ADR was found to improve during SD onset, indicating that DCI was unlikely to occur. Since these metrics were compared to an hour before and after SD onset and there was overlap between SDs, the worsening of ADR may simply have been missed due to the absence of healthy or normal brain activity. Additionally, the relative power of the delta wavelength was shown to be more affected by SD in the stroke patient for all identified SDs. The bypass patient experienced more disturbance and modulation of relative power after SD resolved. These differences can inform on vulnerability of the impacted brain areas and their susceptibility to modulation.

Most research on CFC revolves around theta, delta, alpha, and gamma, with much focus on theta-gamma PAC as it plays a crucial role in memory. In epileptogenic zones (EZ) or seizure onset zones (SOZs), it was found that PAC between HFO amplitudes and theta or alpha phase was significantly higher. Studies also show that delta-gamma PAC or delta-beta PAC can provide insight into locating the SOZs. PAC also is implicated in regulating seizure onset[16–18]. PAC is seen aiding interactions between neurons with similar phase preferences, where the LFOs modulate and promote the HFOs[17]. Little discussion is done on AAC and its relation to seizures, stroke, or other severe brain injuries, however it likely follows a similar trend as PAC does.

There was a slight increase in the MI and PLV during and after SD onset, respectively. For the MI, the delta phase was integral for higher MI values. When the delta phase was impacted, the MI did not solely increase but rather gained a broader spread before returning to baseline. What's interesting is that the LFO amplitudes were found to have a higher MI than the HFO amplitudes when the delta phase was impacted. For the PLV, both the delta and HG phases were integral for higher PLV values. The change in PLV was much more difficult to see in the time series data, but there was a general trend of increasing PLV during SD onset, regardless of SD duration, seen in the regression plots (Figure 12). Both

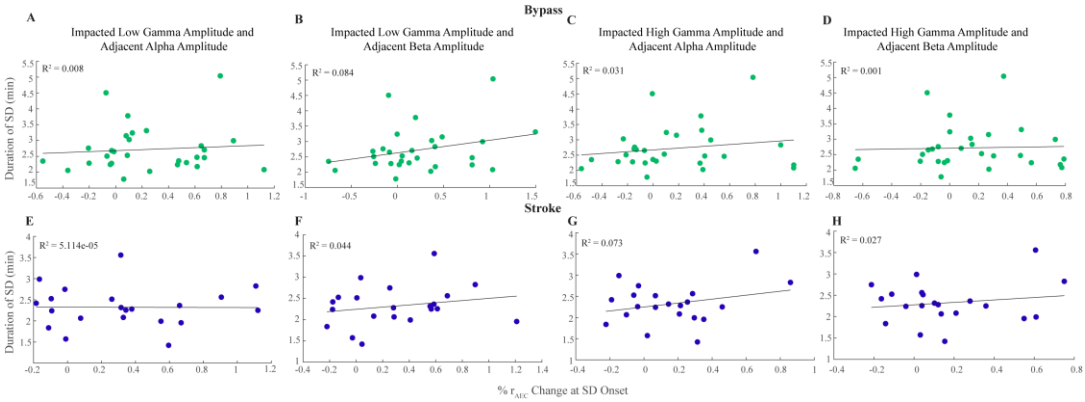

Fig. 16. r_{AEC} Regression Before versus During SD Onset. Correlation between SD duration and percent r_{AEC} change at SD onset is minimal.

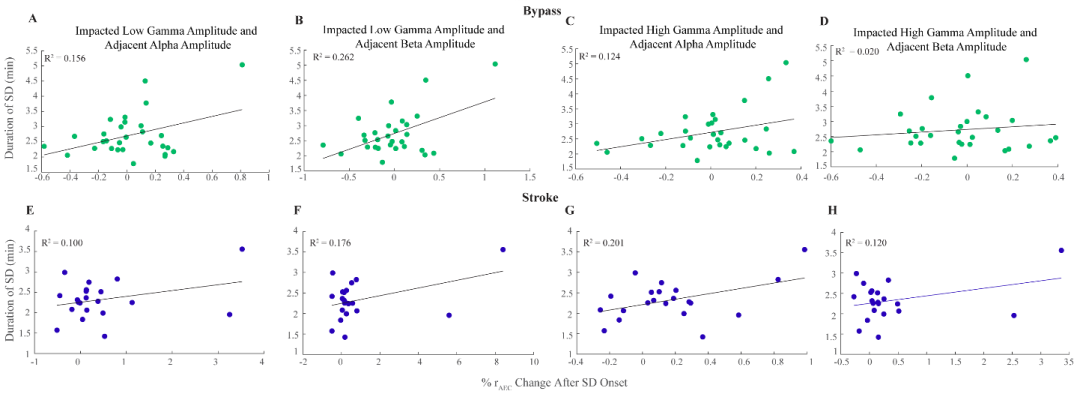

Fig. 17. r_{AEC} Regression During versus After SD Onset. A-D) Correlation between SD duration and percent r_{AEC} change after SD onset is much higher than seen with percent change at SD onset for the bypass patient. E-H) Correlation between SD duration and percent change after SD onset is still very loose and sporadic. There is seemingly less sensible correlation than there was at SD onset.

of these calculations resulted in low-valued reported metrics. Before SD onset, there was little to no PAC found at all, however, after SD onset, PLV found some PAC whilst MI found none. It is assumed that there would be little to no coupling occurring at all in a diseased or injured brain. The discrepancy seen in these metrics may be due to the imperfect sinusoidal oscillation of each brain activity wavelength. This imperfection heavily influences the phase and amplitude found by the Hilbert transform and may explain why the PLV found a higher value after SD onset whilst the MI did not. Additionally, PAC is traditionally done using the HFO amplitude and LFO phases. In this study, there was more PAC when LFO amplitudes were used with the delta or LFO phase. The impact that SDs have on this range of frequencies likely influences the ability of the PAC to occur.

The lack of correlation between MI and SD duration should be investigated further. MI is a fairly standard metric of measuring PAC whilst PLV is still being studied as its rival. There has been argument that PLV may be more beneficial, but no concrete evidence has been shown thus far. With this study, the PLV appeared to be far more affected by SD than MI was. The percent change across time that MI experienced was very minimal, leading to little trend. PLV was shown to have a positive correlation with SD duration and actively changed during SD onset compared to before and after.

The r_{AEC} showed a hike in value during SD onset as well as a rough positive correlation between SD duration and percent change. The impacted gamma amplitude was responsible for higher r_{AEC} values. Adjacent theta, alpha, beta, and LG amplitudes also contributed to the higher r_{AEC} values. This is similar to the PAC found in SOZs, where the HFO amplitude reported higher PAC. More interestingly, the r_{AEC} was affected more after SD resolved, where the r_{AEC} decreased below baseline after SD resolved. This is not too dissimilar to the effect SD has on CBF. With this, the r_{AEC} may be able to perform a similar task as PAC in terms of locating impacted areas.

Across the two patients, subtle differences were observed. The stroke patient showed much more negative relative power of brain frequencies than the bypass patient. More interestingly, the stroke patient reported higher r_{AEC} values across the board whilst incurring very subtle differences otherwise. There is thought that the smaller peak amplitudes and duration of SD may have allowed for better r_{AEC}.

Limitations

Each SD was found by hand through hour-by-hour display of data. Due to the nature of the data, there were many artifacts that either obscured or rendered a visible SD unusable. The resolution of the figures from MATLAB heavily influenced the detection of SD. Many were added after the initial round of identification whilst verifying the adjacent electrodes. Additionally, many electrodes that had SD at one point were used as adjacent electrodes for neighboring impacted electrodes so long as there was no overlapping SD for two hours.

The approach used to calculate CFC in this study presented its own challenges with using an impacted electrode and a non-impacted electrode. The electrodes used in the calculations were not guaranteed to be neighboring when SD was present in three or more neighboring electrodes. The jump in space, despite possibly being only a few millimeters, could have obscured the true value of each metric. Additionally, only one hour of buffer time before and after SD was used. The additional hour may have provided ample time for proper recovery before the next SD occurred, allowing the baseline to return to a more normal state. Similarly, many SDs overlapped or occurred within minutes, thus the before and after SD were not guaranteed to be sin SD.

CFC is incredibly prone to bias. The MI was calculated utilizing a generated surrogate data set, but the other metrics were not. For the MI, the surrogate dataset was generated using segment shuffling. This only partially destroys the time dependency of the time series data. This was done as point shuffling was far too destructive as it removed all time dependency. The length of segment chosen may not have been short enough to remove enough time dependency or it may have been too short

resulting in excessive destruction of the data. Further testing of the shuffled segments needs to be analyzed to ensure validity of the destruction of correlation between time and metric.

Many comorbidities could also influence the results shown in this study. The data was deidentified and the annotations of the dataset were lost for both patients. Specific placement of the electrodes and past medical history of these patients was unknown. Thus, this study was done under the assumption that the only injuries incurred by these patients were of the bypass and the stroke.

Future Direction

More investigation into these metrics will prove beneficial in understanding the effects of SD on the brain. Further investigation into ADR and other similar metrics such as (delta + theta)/(alpha + beta) power ratio or relative alpha variability will help inform on the extent of impact SD has. Figuring out if ADR does increase during SD onset or if that was unique to this study is important. Closer investigation of PAC is also important. The trends seen in this study resemble those of epileptic PAC studies, indicating that there may be other similarities between epileptic patients and patients with SD. Validity of r_{AEC} as an informative metric may provide a way to locate impacted areas of the brain. The linkage between r_{AEC}, CBF, and SD – if any – could also provide a new way of monitoring CBF.

Overall, a more diverse group of patients and intuitive correlations will help show if trends are unique to specific patients or if there are correlations that better encapsulate the effect SD has. Duration of suppression, amplitude of SD, frequency of SD, and spread of SD can all provide more information on the extent of impact SD has.

Materials and Methods

Deidentified ECoG data was obtained from the University of Virginia intensive care unit (ICU). The data was processed using MATLAB. Three filters were used: bandpass (0.5 Hz – 100 Hz), notch or bandstop (60 Hz), and a lowpass (0.01 Hz). The bandpass filtered for the spontaneous brain activity range (0.5 Hz – 30 Hz) whilst also including the gamma band (30 Hz – 100 Hz). The notch filter and lowpass filter performed similar functions to remove noise and identify SD. The lowpass filter revealed slow potential changes (SPC). The baseline was corrected by subtracting the moving median over a period of 10 minutes from each filtered data. This was done using the movmedian function in MATLAB.

SD Identification and Characterization

SDs were identified by a sharp, negative DC shift in both the notch and SPC. The data was viewed an hour at a time and all SDs, SD durations, and durations of high frequency activity suppression were recorded. The SD began immediately before onset and ended immediately after resolvement or return to baseline. The duration of high frequency activity suppression was found similarly. The peak amplitude of SD was found using the min function in MATLAB over the specific time points that SD occurred.

Wavelength Extraction

Bandpass data was further filtered into individual wavelengths: delta (0.98 Hz – 3.91 Hz), theta (4.39 Hz – 7.32 Hz), alpha (7.81 Hz – 12.21 Hz), beta (12.70 Hz – 29.79 Hz), LG (30 Hz – 60 Hz), and HG (60.01 Hz – 100 Hz). The integral of power was calculated over 10 seconds for each frequency range. The ADR was calculated using the integral of power of alpha over the integral of power of delta over a period of 30 seconds. This was done to ensure SD effect was not missed or obscured.

CFC Calculations

The phase and amplitude of each frequency range was extracted using the Hilbert transform in MATLAB. Specifically, the phase was found using the angle function on the Hilbert transform and the amplitude was found using the absolute value of the Hilbert transform. Each metric was calculated using one impacted electrode or electrode with SD and one adjacent or non-impacted electrode. Each metric was calculated for every wavelength and impacted/adjacent combination possible over a period of 2 hours every 30 seconds for 10 trials.

Modulation Index

MI was found using the protocol from Zhang et al. Raw MI was found using the composite signal of the phase of one wavelength and the

$$MI_{raw} = mean\left|a_{SD/adj}(t) \times e^{i \times \Phi_{adj/S}(t)}\right| \quad [1]$$

amplitude of a different wavelength (Equation 1). The surrogate data was generated by using segment shuffling. Five windows of two second segments were chosen. 30 seconds of data were parsed into these windows and randomly shuffled 100 times to generate the surrogate

$$Z_{surr}(t,\tau) = a_{SD/adj}(t + \tau) \times e^{i \times \Phi_{adj/S}(t)} \quad [2]$$

composite signal calculated (Equation 2). The mean and standard deviation of the surrogate composite signal was used to determine the distance that the raw MI was from randomized data (Equation 3). This was done to determine the remove the random chance that the MI found was not biologically relevant[19].

$$MI = \frac{MI_{raw} - \mu}{\sigma} \quad [3]$$

Phase Locking Value

PLV was found using the protocol from Zhang et al. using phases of two different wavelengths where jΔt is the sampling frequency (Equation 4)[19].

$$\text{PLV} = \left|\frac{1}{N}\sum_{j=1}^{N} e^{i[\phi_{SD}(j\Delta t) - \phi_{adj}(j\Delta t)}\right| \quad [4]$$

r_{AEC}

r_{AEC} was found using the protocol from Penny et al. the amplitudes of two different wavelengths (Equation 5).

$$r_{AEC} = Corr_n\left(a_{SD}[n],\ a_{adj}[n]\right) \quad [5]$$

The correlation matrix was found using the standard correlation equation (Equation 6).

Analysis

Median values across trials were used to generate the heatmaps and regression plots. Percent change between before and during SD onset was calculated as the difference between median during and median before over absolute value of the median before (Equation 7).

$$\%\ Change\ at\ SD\ Onset = \frac{median(during) - median(before)}{|median(before)|} \quad [7]$$

Similarly, the percent change between during and after SD onset was calculated as the difference between median during and median after over absolute value of the median after (Equation 8).

$$\%\ Change\ after\ SD\ Onset = \frac{median(during) - median(after)}{|median(after)|} \quad [8]$$

End Matter

Author Contributions and Notes

L.F. designed the research, performed the research, wrote code to process and analyze the data, and wrote the paper.
The author declare no conflict of interest.

Acknowledgments

Special thanks to Dr. Andrew Carlson for his mentorship and the invaluable insight given throughout the course of this project.

References

1. Leao A a. P. Further observations on the spreading depression of activity in the cerebral cortex. *J Neurophysiol*. 1947;10(6):409-414. doi:10.1152/jn.1947.10.6.409
2. Taş YÇ, Solaroğlu İ, Gürsoy-Özdemir Y. Spreading Depolarization Waves in Neurological Diseases: A Short Review about its Pathophysiology and Clinical Relevance. *Curr Neuropharmacol*. 2019;17(2):151-164. doi:10.2174/1570159X15666170915160707
3. Mehra A, Gomez F, Bischof H, Diedrich D, Laudanski K. Cortical Spreading Depolarization and Delayed Cerebral Ischemia; Rethinking Secondary Neurological Injury in Subarachnoid Hemorrhage. *Int J Mol Sci*. 2023;24(12):9883. doi:10.3390/ijms24129883
4. Törteli A, Tóth R, Berger S, et al. Spreading depolarization causes reperfusion failure after cerebral ischemia. *J Cereb Blood Flow Metab*. 2023;43(5):655-664. doi:10.1177/0271678X231153745
5. Dönmez-Demir B, Yemisci M, Uruk G, et al. Cortical spreading depolarization-induced constriction of penetrating arteries can cause watershed ischemia: A potential mechanism for white matter lesions. *J Cereb Blood Flow Metab*. 2023;43(11):1951-1966. doi:10.1177/0271678X231186959
6. Piilgaard H, Lauritzen M. Persistent increase in oxygen consumption and impaired neurovascular coupling after spreading depression in rat neocortex. *J Cereb Blood Flow Metab Off J Int Soc Cereb Blood Flow Metab*. 2009;29(9):1517-1527. doi:10.1038/jcbfm.2009.73
7. Yeh CH, Zhang C, Shi W, Lo MT, Tinkhauser G, Oswal A. Cross-Frequency Coupling and Intelligent Neuromodulation. *Cyborg Bionic Syst*. 2023;4:0034. doi:10.34133/cbsystems.0034
8. Rosenthal ES, Biswal S, Zafar SF, et al. Continuous Electroencephalography Predicts Delayed Cerebral Ischemia after Subarachnoid Hemorrhage: A Prospective Study of Diagnostic Accuracy. *Ann Neurol*. 2018;83(5):958. doi:10.1002/ana.25232
9. Finnigan S, Wong A, Read S. Defining abnormal slow EEG activity in acute ischaemic stroke: Delta/alpha ratio as an optimal QEEG index. *Clin Neurophysiol*. 2016;127(2):1452-1459. doi:10.1016/j.clinph.2015.07.014
10. Wickering E, Gaspard N, Zafar S, et al. Automation of Classical QEEG Trending Methods for Early Detection of Delayed Cerebral Ischemia: More Work to Do. *J Clin Neurophysiol Off Publ Am Electroencephalogr Soc*. 2016;33(3):227-234. doi:10.1097/WNP.0000000000000278
11. Jordan KG. Emergency EEG and continuous EEG monitoring in acute ischemic stroke. *J Clin Neurophysiol Off Publ Am Electroencephalogr Soc*. 2004;21(5):341-352.
12. Aru J, Aru J, Priesemann V, et al. Untangling cross-frequency coupling in neuroscience. *Curr Opin Neurobiol*. 2015;31:51-61. doi:10.1016/j.conb.2014.08.002
13. Bergmann TO, Born J. Phase-Amplitude Coupling: A General Mechanism for Memory Processing and Synaptic Plasticity? *Neuron*. 2018;97(1):10-13. doi:10.1016/j.neuron.2017.12.023
14. Munia TTK, Aviyente S. Time-Frequency Based Phase-Amplitude Coupling Measure For Neuronal Oscillations. *Sci Rep*. 2019;9(1):12441. doi:10.1038/s41598-019-48870-2
15. Penny WD, Duzel E, Miller KJ, Ojemann JG. Testing for nested oscillation. *J Neurosci Methods*. 2008;174(1):50-61. doi:10.1016/j.jneumeth.2008.06.035
16. Yeh CH, Hsin YL. Frequency-frequency coupling of brain oscillations in studying ictal EEG activity. *Brain Stimul Basic Transl Clin Res Neuromodulation*. 2015;8(2):345. doi:10.1016/j.brs.2015.01.115
17. Ma H, Wang Z, Li C, Chen J, Wang Y. Phase–Amplitude Coupling and Epileptogenic Zone Localization of Frontal Epilepsy Based on Intracranial EEG. *Front Neurol*. 2021;12. doi:10.3389/fneur.2021.718683
18. Motoi H, Miyakoshi M, Abel TJ, et al. Phase-amplitude coupling between interictal high-frequency activity and slow waves in epilepsy surgery. *Epilepsia*. 2018;59(10):1954-1965. doi:10.1111/epi.14544
19. Zhang T, Xu X, Zheng C. Reduction in LFP cross-frequency coupling between theta and gamma rhythms associated with impaired STP and LTP in a rat model of brain ischemia. *Front Comput Neurosci*. 2013;7. doi:10.3389/fncom.2013.00027